IEEE Access
Multidisciplinary ⋮ Rapid Review ⋮ Open Access Journal

Received November 9, 2020, accepted November 19, 2020, date of publication November 25, 2020,
date of current version December 9, 2020.

Digital Object Identifier 10.1109/ACCESS.2020.3040701

Design and Characterization of an IQ Reflection-Type Vector Modulator for Ka-Band Using PIN Diodes

RAUL ARRUELA[1,2], (Member, IEEE), DIOGO MARINHO[1,2], (Member, IEEE), TIAGO VARUM[1], (Member, IEEE), AND JOÃO NUNO MATOS[1,2], (Member, IEEE)

[1]Instituto de Telecomunicações, Campus Universitário de Santiago, 3810-193 Aveiro, Portugal
[2]Departamento de Eletrónica, Telecomunicações e Informática, Universidade de Aveiro, 3810-193 Aveiro, Portugal

Corresponding author: Raul Arruela (raul.marques@ua.pt)

This work was supported in part by the Fundação para Ciência e Tecnologia/Ministério da Ciência, Tecnologia e Ensino Superior (FCT/MCTES) through national funds, in part by EU funds under Project UIDB/50008/2020-UIDP/50008/2020, in part by the European Regional Development Fund through the Competitiveness and Internationalization Operational Program, in part by the Regional Operational Program of Lisbon, in part by the Regional Operational Program of the Algarve, in component European Regional Development Fund (FEDER), and in part by the Foundation for Science and Technology, through the Reflectometry Technologies to Enhance the Future Internet of Things and Cyber-Physical Systems (RETIOT) Project, under Grant POCI-01-0145-FEDER-016432.

ABSTRACT Vector modulators (VM) and phase shifters are essential components in phased array antennas with electronic beam steering. This work presents an IQ reflection-type vector modulator using PIN diodes, designed and implemented to operate at 28 GHz. An extensive characterization was carried out, especially concerning bandwidth and input/output return losses. This modulator is capable of producing a 360° phase shifting with a minimum attenuation of 14 dB at 28 GHz, and has a measured bandwidth of 3.6 GHz. A digital control system for the vector modulator was also developed, allowing to obtain pre-selected constellations points, with a measured 0.4 dB of maximum absolute error in amplitude and 2.6° in phase. Additionally, the designed VM was employed in a practical application, where analog beamforming is implemented in a 4×4 transmitter phased array allowing to perform a complete electronic control of the radiation pattern of the array.

INDEX TERMS Vector modulator, phased array, phase shifter, variable attenuator, pin diode, beamforming.

I. INTRODUCTION

Phased Arrays are currently the cornerstone in various technologies using wireless communications, such as 5G, Satellite, or radar systems, in its many applications, from medical imaging to surveillance and security, in military applications or in autonomous vehicles [1]–[6].

A Phased Array Antenna (PAA) consists of an array of radiating elements in which each element can be fed with different phase delays, directing the array's radiation beam. This steering is performed electronically, leading to a faster and more flexible system, and requiring less maintenance than the mechanical systems [7]. Phased Arrays operating in mmWaves meet some important requirements of those systems, enabling low-profile antennas, high bandwidth, and spatial filtering capabilities through electronic beamforming.

The associate editor coordinating the review of this manuscript and approving it for publication was Davide Comite.

Adaptive antennas using beamforming are a technological evolution of phased arrays, which shape and steer the beam of an antenna array, adapting it to the surrounding environment, optimizing the communication. This technology uses sophisticated signal processing techniques to estimate weights, in the form not only of phase differences, but also of relative amplitudes of the signals that feed each element of the array, producing a specific radiation pattern. Beamforming can be implemented in the digital domain (Digital Beamforming), in the analog domain (Analog Beamforming) or in both (Hybrid Beamforming) [8]. Although Digital Beamforming is the most flexible, it may not be suitable for large-scale antenna arrays, because the performance and related costs of the required digital hardware can be a bottleneck. This article focuses on Analog Beamforming.

To deal with the beam direction in a PAA system, it is necessary to control the phase of the signals that feed each element of the antenna array, therefore, it is necessary to use Phase-Shifters (PS) for this. These devices are fundamental

This work is licensed under a Creative Commons Attribution 4.0 License. For more information, see https://creativecommons.org/licenses/by/4.0/

in modern and smart systems, and are subject to a great attention and research, looking for more versatile, compact, and efficient solutions, suitable to antenna array systems. Additionally, in the more evolved architectures using beamforming, variable amplifiers or attenuators are still needed.

These components can be implemented in different stages of a transceiver, in baseband (BB), in the intermediate-frequency (IF) stage, at the local-oscillator (LO) unit, or in the radio frequency (RF) part. However, when implemented in RF, there is the advantage of using less mixers, eliminating the need of a mixer per element. It is in this sense that a lot of research and many solutions have been developed, given the simplicity and potential low cost that the implementation in RF offers, especially in large-scale antenna arrays.

Phase shifters can be passive or active [9]. The passive PS offers more linearity and zero DC power consumption, and the most common structures are the Loaded-Line Phase Shifter [10], [11], the Switched-Delay Lines Phase Shifter [12] and the Reflection-Type Phase Shifter (RTPS) [13]–[16]. In some reports, limitations were identified regarding, for example, the range of phase variation, or even because some are inherently digital (Switched-Delay Lines) and do not allow a continuous phase shift. The RTPS stands out among these solutions. It consists of a 90° hybrid coupler where reactive terminations are applied, such as variable capacitors (varactors) or variable inductors, allowing phase shifting.

Three decades ago, Devlin and Minnis [17] presented a new concept by modifying the above mentioned RTPS structure, replacing the variable capacitors (or inductors) by Field-Effect Transistors (FET's) functioning as variable resistors (cold transistors) and thus obtaining a Reflection-Type Bi-phase Variable Attenuator (RTBVA). With two RTBVA's operating in quadrature, they implemented the first IQ Reflection Type Vector Modulator (IQ-RTVM), which allowed the ability to control not only the phase in a 360° range, but also the amplitude [18], simultaneously. Since then, this new structure has received a lot of interest, given the importance it has for mmWaves Phased Arrays and also in direct modulation transmitters [19]–[22].

Several versions concerning the structure of a vector modulator have been reported, where most of them are carried out through integrated circuits. In [19] is presented a 30 - 40 GHz MMIC IQ vector Modulator with pHEMT transistors functioning as variable resistors, with 5 dB of minimum insertion loss, ±2° phase error and ±0.3 dB amplitude imbalance. In [20] the authors show a much wideband IQ vector modulator, made in a 0.13 μm CMOS process, with 20 - 40 GHz frequency range, less than 13 dB of minimum insertion loss and modulation bandwidth larger than 1 GHz. A BPSK modulator in a MMIC GaAs process is shown in [22] where even higher bandwidth (40 GHz) is achieved, from 25 to 65 GHz, modulation bandwidth greater than 500 MHz, minimum insertion loss less than 10 dB, less than 6° of phase imbalance and less than 0.9 dB of amplitude imbalance.

In some reports, the authors present different techniques to deal with the negative effects caused by parasitic elements in the transistors, such as balanced configurations [19], [23], the use of bond-wire parasitic inductance [24] and also the introduction of series inductance and shunt resistor [25]. Unfortunately, there are only a few versions implemented in Printed Circuit Board (PCB) for K/Ka band reported in literature. In [26] and [7], the authors present a phased array radar for 24 GHz, implementing an IQ-RTVM using a RTBVA with PIN diodes [27] as a variable resistance element. They achieved a phase variation range of 360° and a minimum 10 dB insertion loss.

To the best of our knowledge, no work has been reported, where a broader characterization has been made on IQ- RTVM's PIN diodes based, especially focusing on the frequency bandwidth, and the variation of reflection coefficient at input/output ports as a function of S_{21}. In this work a microstrip IQ-RTVM was designed, implemented, and extensively characterized, using PIN diodes, and operating in the K/Ka band.

The constellation of IQ points obtained through S_{21} parameter over the frequency is provided, as well as the minimum attenuation as a function of frequency (with 360° of variation range), thus obtaining the 3-dB bandwidth. It is also possible to observe how the return loss at input/output ports varies with the attenuation of the modulator, for different frequencies. An electronic circuit devoted to the digital control unit for the modulator was created. Finally, to demonstrate the functionality and applicability of this system, an experimental test was carried out on a 28 GHz, 4 × 4 transmitter phased array.

This document is organized as follows. Section I introduces the work, provides a brief description of the state-of-the-art, and presents the main objectives. In section II a theoretical introduction to IQ-RTVM is made, starting by explaining the reflection-type bi-phase variable attenuator. Next, the integration of two RTBVA resulting in a reflection-type IQ vector modulator is explained, and finally the implemented circuit is presented. The digital control circuit is described in section III and the modulator's characterization is shown in section IV. A practical application is presented in section V with measurement results and finally, in section VI the main conclusions are taken.

II. VM ANALYSIS AND DESIGN

The vector modulator concept is based on the mathematical principle which states that a vector v is the sum of its orthogonal components I and Q, as illustrated in Fig. 1.

As can be seen in Fig. 2, in a vector modulator two orthogonal signals are created from an input signal x(t) through a 90° splitter and, before adding them to obtain y(t), these components are properly attenuated, resulting in a signal at the output port that is a replica of x(t) scaled by a factor A and a phase change of ϕ.

Equations (1) to (3) demonstrate the relationship between the input and output of the vector modulator when the circuit

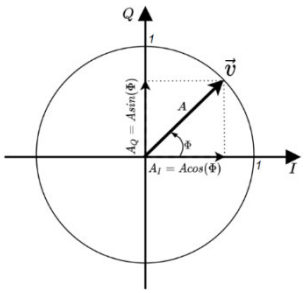

FIGURE 1. A vector (v) decomposed into two orthogonal components.

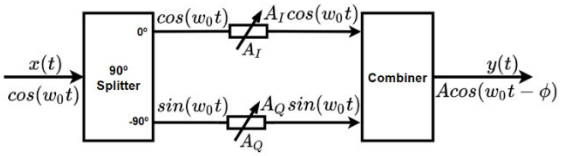

FIGURE 2. Vector modulator block diagram.

is excited by a sinusoidal signal $x(t) = \cos(w_0 t)$

$$\begin{aligned} y(t) &= A_I \cos(w_0 t) + A_Q \sin(w_0 t) \\ &= \sqrt{A_I^2 + A_Q^2} \cos\left(w_0 t - arctg\left(\frac{A_Q}{A_I}\right)\right) \\ &= A\cos(w_0 t - \phi). \end{aligned} \tag{1}$$

Being,

$$A = \sqrt{A_I^2 + A_Q^2} \,(2) \tag{2}$$

$$\phi = \arctan\left(\frac{A_Q}{A_I}\right). \tag{3}$$

A. REFLECTION-TYPE BI-PHASE VARIABLE ATTENUATOR

An RTBVA is illustrated in Fig. 3 and consists of a 90° hybrid coupler and two variable resistors. The input port of the attenuator is the input of the hybrid (port 1) and the output is the isolation port (port 2). The resistance of the two variable resistors are always identical and are connected to the transmission ports 3 and 4, which are 90 degrees delayed.

Assuming a characteristic impedance of $Z_0 = 50\ \Omega$, the operating principle can be explained as follows. When the resistors have 50 Ω value, $\Gamma_t = 0$, ports 3 and 4 (-90° and 0° respectively) are matched, therefore, the signal applied at the input will be completely dissipated in the resistors and no signal will reach the output. The resistors can be varied between 0 Ω and Rmax (where Rmax≫50 Ω). As soon as the resistor value is changed from 50 Ω, the reflection coefficient Γ_t is no longer zero and will tend to −1 if the resistor value tends to 0 Ω, and to 1 if the resistor value tends to Rmax, resulting in a reflected signal from the resistors and forwarded to the output port (i.e. to the isolation port).

Note that according to (4), the reflection coefficient of the resistors changes the signal around 50 Ω, which will cause a phase inversion in the output port signal.

$$\Gamma_t = \frac{Z_t - Z_0}{Z_t + Z_0} \tag{4}$$

The S-parameters of the RTBVA can be obtained from the S-parameter matrix of an ideal 90° hybrid coupler (with ports numbered accordingly to Fig.3).

$$\begin{bmatrix} V_1^- \\ V_2^- \\ V_3^- \\ V_4^- \end{bmatrix} = -\frac{1}{\sqrt{2}} \begin{bmatrix} 0 & 0 & 1 & j \\ 0 & 0 & j & 1 \\ 1 & j & 0 & 0 \\ j & 1 & 0 & 0 \end{bmatrix} \begin{bmatrix} V_1^+ \\ V_2^+ \\ V_3^+ \\ V_4^+ \end{bmatrix} \tag{5}$$

To obtain the S_{21} we simply solve the equation for $\frac{V_2^-}{V_1^+}$ and, knowing that $\Gamma_t = \frac{V_3^+}{V_3^-} = \frac{V_4^+}{V_4^-}$, it gives

$$S_{21} = j\Gamma_t \tag{6}$$

$$|S_{21}| = |\Gamma_t| \tag{7}$$

$$\angle S_{21} = \frac{\pi}{2} sign(\Gamma_t). \tag{8}$$

The S_{11} is obtained solving (5) for $\frac{V_1^-}{V_1^+}$ and, with the knowledge that $V_3^+ = -jV_4^+$, we get

$$S_{11} = 0. \tag{9}$$

Lastly, S_{22} is also zero, which can be inferred by the symmetry of the circuit. In Fig. 4 it's possible to observe the results of a RTBVA simulation with ideal components.

Regarding the variable resistance, among the various options available, PIN diodes were chosen since despite they

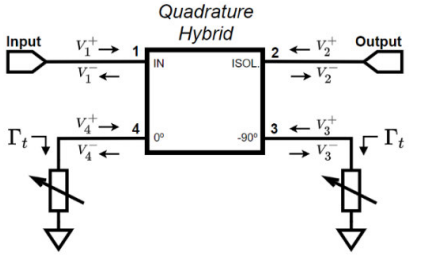

FIGURE 3. Reflection type bi-phase variable attenuator block diagram.

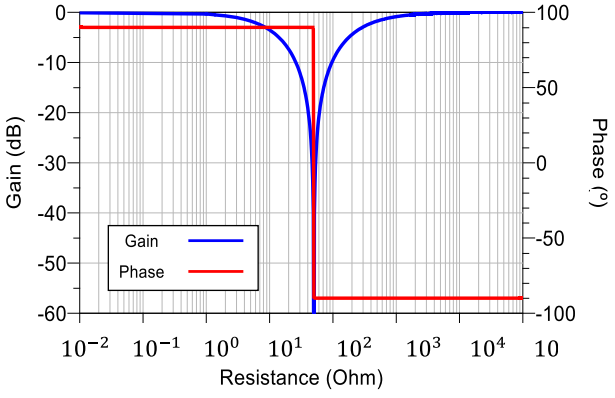

FIGURE 4. Simulated RTBVA: attenuation and phase response.

work as a typical diode when operating at low frequencies, at high frequencies they behave like a resistor. In this work, the MA4PBL027 [28], a MACOM silicon beam PIN diode, was used. This diode has low parasitic elements (series resistance, capacitance, and inductance), a fast switching speed, low insertion loss, and high isolation, making it highly recommended for use in microwave and millimeter wave designs. Fig. 5 shows the equivalent model of the PIN diode for high frequencies when forward biased. The intrinsic parasitic values correspond to a maximum series resistance of 4.0 Ω, a series inductance of 0.15 nH and a total capacitance (Cj+Cp) of 0.04 pF. Typically, for a bias voltage ranging from 0.9 V to 0.4 V, the intrinsic resistance ranges from 0 Ω to Rmax.

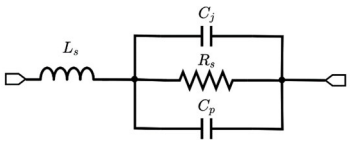

FIGURE 5. PIN diode high-frequency model.

However, as seen in the model, it has parasitic elements, such as capacitors and inductors that will contribute to a performance degradation of the attenuator. In fact, other non-idealities, such as the non-zero hybrid insertion loss, or if the resistors limits may not be exactly 0 Ω and Rmax, certainly will introduce losses in the RTBVA causing a minimum non-zero attenuation and a limit on the maximum attenuation possible, between its input and output, as well as some phase variation.

B. IQ REFLECTION-TYPE VECTOR MODULATOR

The appropriate combination of two RTBVA's, using an additional quadrature hybrid coupler and a power combiner, results in an IQ-Reflection Type Vector Modulator, as illustrated in Fig. 6.

The operation concept of this structure implies that the input signal is divided by the hybrid coupler into two orthogonal signals, the I and Q components, which are then applied to the respective RTBVA. These attenuators will in turn modulate each signal component in amplitude and, eventually a phase inversion will occur, depending on the value of the variable resistances of the RTBVA.

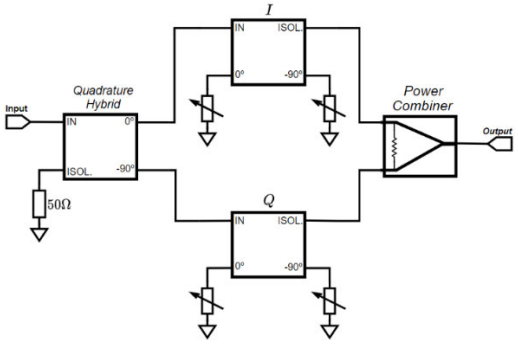

FIGURE 6. IQ-reflection type vector modulator block diagram.

Then, the two quadrature signals are added in the power combiner, thus obtaining an IQ vector modulator capable of changing the phase and amplitude of the input signal in a 360° range with an attenuation factor between 0 and 1. Therefore, considering the attenuation in each RTBVA as A_I and A_Q respectively, an input signal applied to the IQ-RTVM, will appear at the output with a gain factor A (2) and a phase shifting ϕ (3).

C. IQ-RTVM DESIGN

The vector modulator was designed on a RO4350B substrate (thickness 0.254 mm) using microstrip technology. The circuit is mainly composed by three 90° hybrid couplers, a Wilkinson power combiner and four PIN diodes. The layout of the designed IQ-RTVM is shown in Fig. 7.

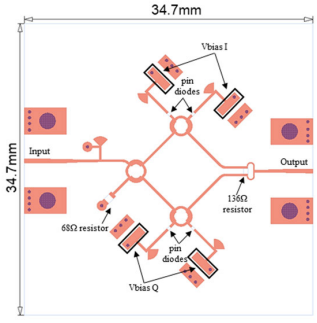

FIGURE 7. Layout of the designed IQ vector modulator.

The circuit was designed based on lines with characteristic impedance of $Z_0 = 68\ \Omega$. This Z_0 was selected to achieve a reasonable ratio between the length and width of the lines in the circular couplers. Additionally, their circular shape optimizes the functionality and avoid undesirable coupling.

Nevertheless, two quarter-wavelength microstrip transformers were placed at the input and output to match the ports to 50 Ω. The bias circuits include a radial stub followed by a 180° transmission line in order to guarantee sufficient distance between the diode and the DC voltage pad and, simultaneously, a short circuit for the signal at 28 GHz. The global dimensions of the fabricated PCB of the designed vector modulator are 34.7mm×34.7mm. In Fig. 8 a photograph of the fabricated VM is shown.

III. DIGITAL CONTROLLER

The variable resistors, that allow to perform the RTBVA, and enable the operation of the vector modulator, are controlled through a digital controlled system whose block diagram is shown in Fig. 9. In this unit, the different bias voltages are created which are then applied to the various forward biased PIN diodes.

The microcontroller unit (Arduino Uno was used) is controlled by the PC through a USB connection. A Digital-to-Analog (DAC) module was developed with four DACs,

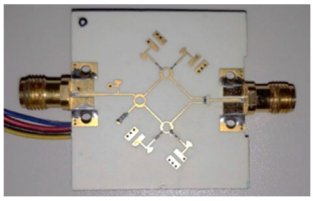

FIGURE 8. Photograph of the IQ vector modulator prototype.

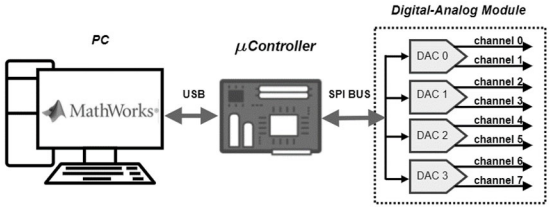

FIGURE 9. Block diagram of the digital controller system.

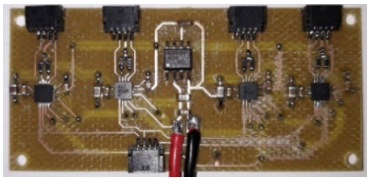

FIGURE 10. Photograph of the 8-channel Digital-Analog module.

each DAC has two independent outputs that are going to produce eight bias voltages for the diodes of the vector modulators. There is a four-wire SPI (serial peripheral interface) connection between the microcontroller and the DAC module, to control the voltages at their output channels. The photograph of the developed PCB of the digital-analog module is shown in Fig. 10, which is going to control four vector modulators. Each one of the four DACs has two outputs to control one VM, resulting in eight different bias voltages. This module makes use of an IC voltage regulator MAX6161AESA+ [29] and four DACs MAX5550 [30] from Maxim Integrated supplier, connected in Daisy-Chain mode which results in simplified layout of the PCB and less number of connections to the microcontroller. This DAC has 10 bits of resolution and allows to operate with SPI or I2C protocol, with a sampling frequency of 10 Msps and 400 Ksps, respectively. The higher the resolution of the DAC, the higher the resolution of the control voltage of the PIN diodes biasing and, therefore, the higher the resolution of the VM phase and amplitude control. Likewise, the higher the sample rate, the faster the beam can be steering.

IV. MEASUREMENT RESULTS

The vector modulator was extensively measured and characterized in terms of its principal aspects that affects its performance. Fig. 11 shows a group of four constellations obtained at different frequencies, 24, 26.1, 28 and 30 GHz respectively, where each point of the constellation represents the S_{21} parameter (i.e. the phase shifting and attenuation of the modulator) for a given pair of bias voltage $\left(V_I, V_Q\right)$.

In addition, red circles of constant gain are exhibited, representing the minimum attenuation with points in all quadrants (i.e. in a 360° range). According to Fig. 11 c), this modulator provides a minimum attenuation of 12.6 dB at 26.1 GHz within a 360° range. Fig. 12 presents the variation of the vector modulator gain (maximum value within a 360° range) over a wide range of frequencies. It is possible to observe an obtained bandwidth of 3.6 GHz, assuming the range where the gain falls 3 dB. This result makes this VM usable in a wide frequency range (from 24.7 to 28.3 GHz).

The modulator was characterized also in terms of return loss at its input and output port, and the results are shown in Fig. 13 and Fig. 14, respectively, where each point represents the return loss for a given pair of bias voltage $\left(V_I, V_Q\right)$.

It is possible to observe that, at 28 GHz, the modulator presents the best performance regarding the return loss in both ports. Additionally, as can be seen from Fig. 13, the constellation of points corresponding to 24, 26 and 28 GHz attains an input return loss higher than 10 dB, which shows that the input is (considerably well) matched at those frequencies too.

It is also possible to observe that the variation of the output return loss is higher than that from the input, with a 15 dB of maximum variation, at 28 GHz. The explanation for the difference between the two ports may lie in the fact that at input a 90° hybrid coupler is used and at output a Wilkinson combiner is used instead, which due to their different properties makes the circuit asymmetric. Fig. 15 shows the constellation points obtained at 28 GHz where the digital controller was set to obtain a 16 dB attenuation with 10° steps, in 5 consecutive repetitions (185 datapoints). A maximum absolute error of 0.2 dB in amplitude and 1.9° in phase was measured.

Fig. 16 shows the result from 5° steps (with no repetitions), resulting in 0.4 dB max. absolute error in amplitude and 2.6° in phase. A performance comparison with previous works is shown in Table 1.

V. IQ-RTVM'S BEAMFORMING APPLICATION

To validate the application of these vector modulators in a practical application, it was planned a setup to reproduce a beam steering scenario, which is illustrated in the block diagram of the Fig. 18. It is composed by a baseband processing unit which includes a USRP (Universal Software Radio Peripheral), a Host-PC, and a digital control circuit, responsible to control the DC bias of each vector modulator. The operating frequency was selected in the Ka-band, at 28 GHz.

The system comprehends four channels for transmission and for reception, connecting one USRP output IF signal (at 3.84 GHz) to a power splitter, and then to a 4 × 4 series-fed antenna array (with four independent linear sub-arrays) [31], through a set of RF links composed of Upconverters and Downconverters units, and the designed IQ-RTVM.

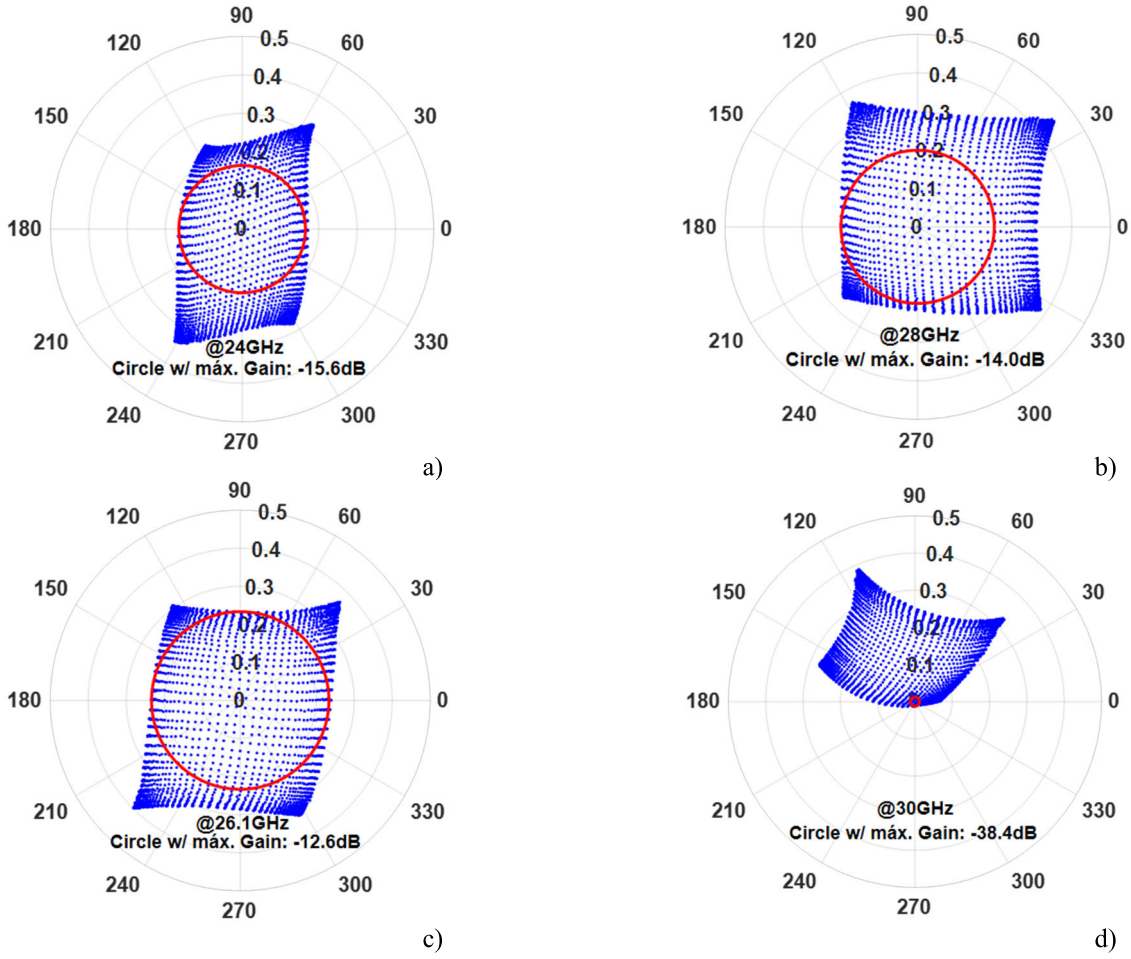

FIGURE 11. S_{21} constellation and the maximum gain circles at various frequencies a) 24 GHz, b) 28 GHz, c) 26.1 GHz and d) 30 GHz.

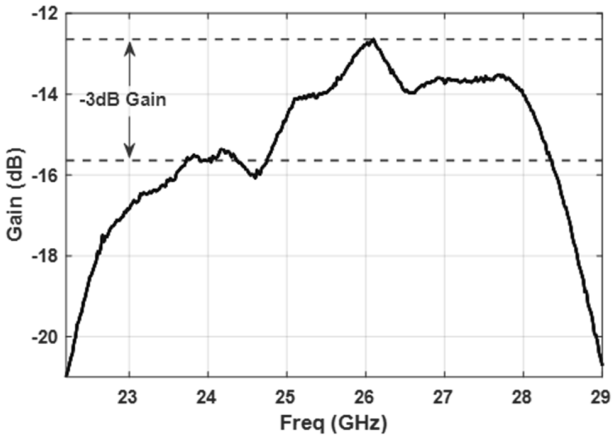

FIGURE 12. Vector modulator gain over frequency.

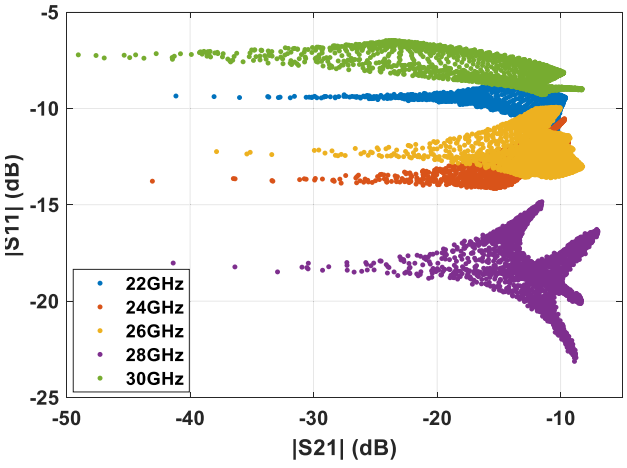

FIGURE 13. Return loss at the input port as a function of S_{21}, obtained at various frequencies.

The four RF Upconverters modules translates the IF frequency (3.84 GHz) to 28 GHz, which are then modulated in terms of amplitude and phase using the vector modulator, while the four Downconverters converts the received 28 GHz signals to IF signals to be processed in the USRP unit, that is responsible for the demodulation and execute all the remain baseband processing of the received samples.

The measurement setup is shown in Fig. 17 and includes a power supply that provides the DC voltage to the Up/Down converters, one PLL (Phase Locked Loop) generating a 12.08 GHz LO signal, a power splitter that divides the IF signal into four channels, and applies them to input of the

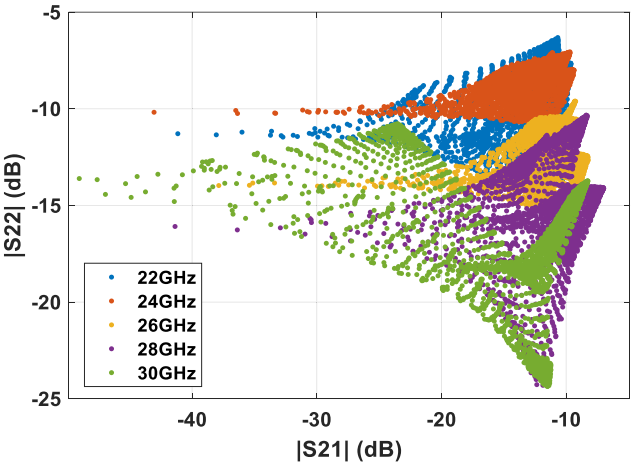

FIGURE 14. Return loss at the output port as a function of S_{21}, obtained at various frequencies.

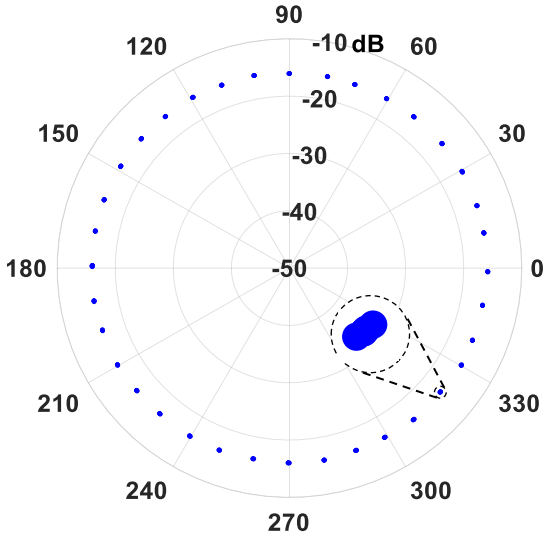

FIGURE 15. S_{21} - 10° step points with 16 dB attenuation, obtained with the vector modulator digital controller (5 repetitions).

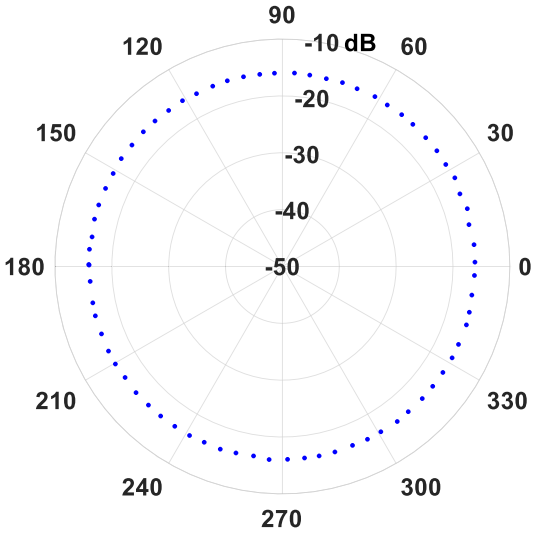

FIGURE 16. S_{21} - 5° step points with 16 dB attenuation, obtained with the vector modulator digital controller.

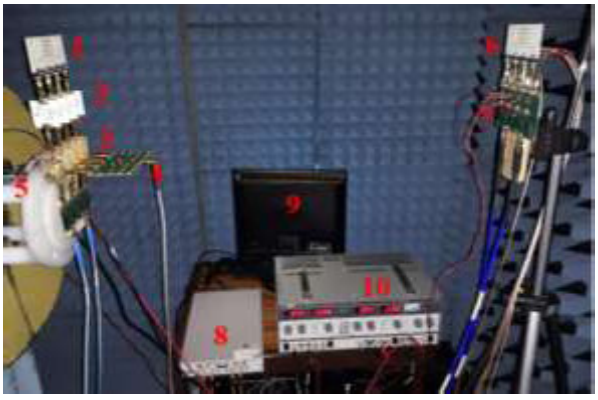

FIGURE 17. Photograph of the experimental setup (1-Tx antenna array, 2-Vector Modulators, 3-Upconverters, 4-Power Splitter, 5-Digital Control Module, 6-Rx antenna array, 7-Downconverters, 8-USRP N310, 9-PC, 10-Power Supply).

upconverters, two antenna arrays, a USRP that generates one IF and receive four IF signals, four vector modulators and an 8-channel Digital-Analog module. All these components can be identified in Fig. 17.

Before starting the measurement process, a simple calibration was made to ensure that the signals arriving to the receiver antenna array were all in phase. In this work, the beamforming was performed on the transmitter side. The Tx array antenna was carefully positioned in the rotor arm of the anechoic chamber. The receiving antenna has the important function of reading the radiation pattern from the transmitter and was placed in far field (65 cm away from the transmitter).

The beamforming concept is easily understandable, and it consists in manipulating the radiation pattern of the antenna array by changing the amplitude and phase of each signal that feeds the antenna. To highlight the vector modulator functionality in beamforming scenario, it was applied a simple progressive phase delay to each Tx channel given by,

$$\alpha = kd\ cos\theta \tag{10}$$

where θ is the desired radiation direction of the antenna array, k=$(2\pi/\lambda)$ and d the distance between elements of the array. The Table 2 represents the estimated phase delay for each channel, considering a set of chosen locations (θ). The beamforming angle was changed in the range $-40°$ to $40°$ with 1-degree step using the vector modulator and for each step it was measured the amplitude of the received signal. An identical process was applied for nine positions of the transmitter.

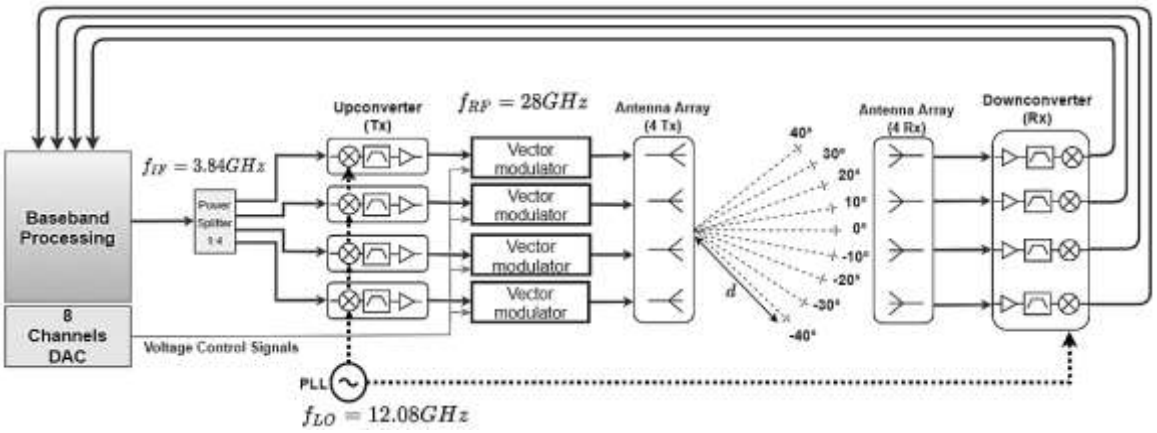

FIGURE 18. Block diagram of the beamforming application setup.

TABLE 1. Performance Comparison With Previous Works.

Reference	[19]	[20]	[22]	[26]	This work
Technology	MMIC pHEMT	0.13µm CMOS	MMIC GaAs	PCB	**PCB**
Type	IQ	IQ	BPSK	IQ	**IQ**
Frequency (GHz)	30-40	20-40	25-65	23.75	**24.7-28.3**
Modulation Bandwidth (GHz)	-	> 1	> 0.5	-	-
Minimum Insertion Loss (dB)	5	< 13	< 10	10	**9***
Others	±2° phase error ±0.3dB ampl. imb.	-	< 6° phase imb. < 0.9dB amp. imb.	-	**< 2.6° phase error < 0.4dB amp. error**

* Note that for beamforming applications (as it is in this case), 14 dB should be considered instead of 9 dB, this is because a 360° phase shift range with constant insertion loss is required in most cases (see the red circle in Fig. 11b). But, for a fair comparison, in the table we put 9 dB.

TABLE 2. Beamforming Phase Weights.

Steering Angle θ	α_1	α_2	α_3	α_4
40°	0°	173°	346°	519°
30°	0°	135°	270°	405°
20°	0°	92°	184°	276°
10°	0°	47°	94°	141°
0°	0°	0°	0°	0°
-10°	0°	-47°	-94°	-141°
-20°	0°	-92°	-184°	-276°
-30°	0°	-135°	-270°	-405°
-40	0°	-173°	-347°	-519°

The measurement results of the radiation patterns are shown in Fig. 19, and a good agreement between the desired angle of the beam (θ) and the maximum value of the antenna radiation is observable.

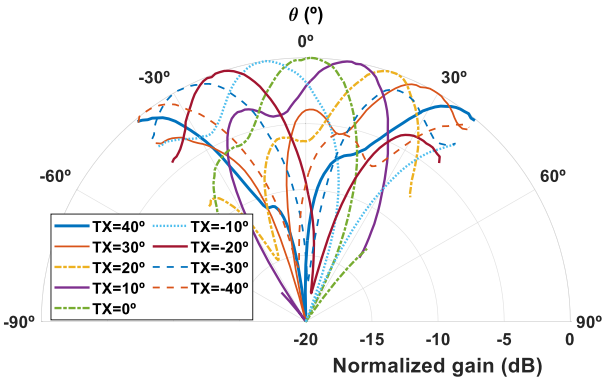

FIGURE 19. Beam steering measured results at 28 GHz.

VI. CONCLUSION

In this work, an IQ vector modulator operating at 28 GHz using PIN diodes was designed and implemented in PCB. The vector modulator was extensively characterized, with respect to bandwidth and return loss. A 3-dB bandwidth of 3.6 GHz and a minimum attenuation (with 360° of phase shift range) of −14 dB at 28 GHz, and −12.6 dB at 26.1 GHz, were measured. A digital control circuit was developed and two constellations with phase differences of 10° and 5° between consecutive points were demonstrated. An amplitude error of 0.4 dB and a phase error of 2.6° was measured. An experimental beamforming application was also shown to demonstrate and validate the vector modulator.

REFERENCES

[1] W. Hong, K.-H. Baek, Y. Lee, Y. Kim, and S.-T. Ko, "Study and prototyping of practically large-scale mmWave antenna systems for 5G cellular devices," *IEEE Commun. Mag.*, vol. 52, no. 9, pp. 63–69, Sep. 2014.

[2] W. Hong, Z. H. Jiang, C. Yu, J. Zhou, P. Chen, Z. Yu, H. Zhang, B. Yang, X. Pang, M. Jiang, Y. Cheng, M. K. T. Al-Nuaimi, Y. Zhang, J. Chen, and S. He, "Multibeam antenna technologies for 5G wireless communications," *IEEE Trans. Antennas Propag.*, vol. 65, no. 12, pp. 6231–6249, Dec. 2017.

[3] B. Sadhu, Y. Tousi, J. Hallin, and S. Sahl, "A 28-GHz 32-element TRX phased-array IC with concurrent dual-polarized operation and orthogonal phase and gain control for 5G communications," *IEEE J. Solid-State Circuits*, vol. 52, no. 12, pp. 3373–3391, Dec. 2017.

[4] K. Kibaroglu, M. Sayginer, and G. M. Rebeiz, "A low-cost scalable 32-element 28-GHz phased array transceiver for 5G communication links based on a 2×2 beamformer flip-chip unit cell," *IEEE J. Solid-State Circuits*, vol. 53, no. 5, pp. 1260–1274, May 2018.

[5] G. M. Rebeiz and L. M. Paulsen, "Advances in SATCOM phased arrays using silicon technologies," in *IEEE MTT-S Int. Microw. Symp. Dig.*, Jun. 2017, pp. 1877–1879.

[6] T. Hall, B. T. Nukala, C. Stout, N. Brewer, J. Tsay, J. Lopez, R. E. Banister, T. Nguyen, and D. Y. C. Lie, "A phased array non-contact vital signs sensor with automatic beam steering," in *IEEE MTT-S Int. Microw. Symp. Dig.*, May 2015, pp. 1–4. [Online]. Available: https://ieeexplore.ieee.org/abstract/document/7166973

[7] Z. Peng, L. Ran, and C. Li, "A 24-GHz low-cost continuous beam steering phased array for indoor smart radar," in *Proc. IEEE 58th Int. Midwest Symp. Circuits Syst. (MWSCAS)*, Aug. 2015, pp. 1–4.

[8] I. Ahmed, H. Khammari, A. Shahid, A. Musa, K. S. Kim, E. De Poorter, and I. Moerman, "A survey on hybrid beamforming techniques in 5G: Architecture and system model perspectives," *IEEE Commun. Surveys Tuts.*, vol. 20, no. 4, pp. 3060–3097, 4th Quart., 2018.

[9] H. Jia, L. Kuang, W. Zhu, Z. Wang, F. Ma, Z. Wang, and B. Chi, "A 77 GHz frequency doubling two-path phased-array FMCW transceiver for automotive radar," *IEEE J. Solid-State Circuits*, vol. 51, no. 10, pp. 2299–2311, Oct. 2016.

[10] S. Barker and G. M. Rebeiz, "Distributed MEMS true-time delay phase shifters and wide-band switches," *IEEE Trans. Microw. Theory Techn.*, vol. 46, no. 11, pp. 1881–1890, Nov. 1998.

[11] A. S. Nagra and R. A. York, "Distributed analog phase shifters with low insertion loss," *IEEE Trans. Microw. Theory Techn.*, vol. 47, no. 9, pp. 1705–1711, Sep. 1999.

[12] B. Pillans, S. Eshelman, A. Malczewski, J. Ehmke, and C. Goldsmith, "Ka-band RF MEMS phase shifters," *IEEE Microw. Guided Wave Lett.*, vol. 9, no. 12, pp. 520–522, Dec. 1999.

[13] C. S. Lin, S. F. Chang, and W. C. Hsiao, "A full-360° reflection-type phase shifter with constant insertion loss," *IEEE Microw. Wireless Compon. Lett.*, vol. 18, no. 2, pp. 106–108, Feb. 2008.

[14] N. Mazor, O. Katz, R. Ben-Yishay, D. Liu, A. V. Garcia, and D. Elad, "SiGe based ka-band reflection type phase shifter for integrated phased array transceivers," in *IEEE MTT-S Int. Microw. Symp. Dig.*, May 2016, pp. 31–34.

[15] T. Li, S. Member, H. Wang, and S. Member, "A millimeter-wave fully integrated passive reflection-type phase shifter with transformer-based multi-resonance loads for 360° phase shifting," *IEEE Trans. Circuits Syst. I, Reg. Papers*, vol. 65, no. 4, pp. 1406–1419, Apr. 2018.

[16] R. Garg and A. S. Natarajan, "A 28-GHz low-power phased-array receiver front-end with 360° RTPS phase shift range," *IEEE Trans. Microw. Theory Techn.*, vol. 65, no. 11, pp. 4703–4714, Nov. 2017.

[17] L. M. Devlin and B. J. Minnis, "A versatile vector modulator design for MMIC," in *IEEE Int. Dig. Microw. Symp.*, 1990, pp. 519–521.

[18] M. Tuckman, "I-Q vector modulator—The ideal control component?" *Microw. Syst. News*, pp. 105–115, 1988.

[19] A. E. Ashtiani, S.-I. Nam, A. d'Espona, S. Lucyszyn, and I. D. Robertson, "Direct multilevel carrier modulation using millimeter-wave balanced vector modulators," *IEEE Trans. Microw. Theory Techn.*, vol. 46, no. 12, pp. 2611–2619, Dec. 1998.

[20] H.-Y. Chang, P.-S. Wu, T.-W. Huang, H. Wang, C.-L. Chang, and J. G. J. Chern, "Design and analysis of CMOS broad-band compact high-linearity modulators for gigabit microwave/millimeter-wave applications," *IEEE Trans. Microw. Theory Techn.*, vol. 54, no. 1, pp. 20–30, Jan. 2006.

[21] D. Sun, Y. Fan, J. Xu, and S. Jiang, "A balanced reflection type HMIC vector modulator over 34–36GHz based on cold state pHEMTs," in *Proc. IEEE Int. Wireless Symp. (IWS)*, no. 2, Mar./Apr. 2015, pp. 21–24.

[22] X. Lin, H. Liu, H. Chang, and Y. Wang, "A 25–65 GHz broadband low-LO-driving wide-modulation-bandwidth monolithic BPSK modulator in GaAs PIN diode MMIC process," in *Proc. IEEE Asia–Pacific Microw. Conf. (APMC)*, Nov. 2017, pp. 910–913.

[23] F. Tabarani and H. Schumacher, "0.25 μm SiGe BiCMOS 30GHz balanced vector modulator," in *Proc. IEEE 16th Top. Meeting Silicon Monolithic Integr. Circuits RF Syst. (SiRF)*, no. 4, Jan. 2016, pp. 94–96.

[24] C. Chen, U. Dilshad, G. Mehdi, C. Wang, A. Hu, and J. Miao, "Performance improvement of microwave vector modulator through coupler characteristic impedance optimization and bond-wire inductance utilization," *IEEE Access*, vol. 7, pp. 6151–6160, 2019.

[25] M. Chongcheawchamnan, S. Bunnjaweht, D. Kpogla, D. Lee, and I. D. Robertson, "Microwave I-Q vector modulator using a simple technique for compensation of FET parasitics," *IEEE Trans. Microw. Theory Techn.*, vol. 50, no. 6, pp. 1642–1646, Jun. 2002.

[26] Z. Peng, L. Ran, and C. Li, "A *K*-band portable FMCW radar with beamforming array for short-range localization and vital-Doppler targets discrimination," *IEEE Trans. Microw. Theory Techn.*, vol. 65, no. 9, pp. 3443–3452, Sep. 2017.

[27] W.-T. Kang, I.-S. Chang, and M.-S. Kang, "Reflection-type low-phase-shift attenuator," *IEEE Trans. Microw. Theory Techn.*, vol. 46, no. 7, pp. 1019–1021, Jul. 1998.

[28] *PIN Diode MA4PBL027 MACOM*. Accessed: Jul. 30, 2020. [Online]. Available: https://cdn.macom.com/datasheets/MA4PBL027

[29] *Power Supply MAX6161 Maxim Integrated*. Accessed: Jul. 30, 2020. [Online]. Available: https://datasheets.maximintegrated.com/en/ds/MAX6161-MAX6168.pdf

[30] *DAC MAX5550 Maxim Integrated*. Accessed: Jul. 30, 2020. [Online]. Available: https://datasheets.maximintegrated.com/en/ds/MAX5550.pdf

[31] T. Varum, A. Ramos, and J. N. Matos, "Planar microstrip series-fed array for 5G applications with beamforming capabilities," in *IEEE MTT-S Int. Microw. Symp. Dig.*, Aug. 2018, pp. 1–3.

RAUL ARRUELA (Member, IEEE) was born in Portugal in 1982. He received the M.Sc. degree in electronic and telecommunications engineering from the Universidade de Aveiro, Aveiro, Portugal, in 2018, where he is currently pursuing the Ph.D. degree in electrical engineering with the Department of Electronics, Telecommunications and Informatics. In September 2018, he joined the Instituto de Telecomunicações. His research interests include RF frontends, analog/hybrid beamforming, mmWave, power amplifiers, radar, 5G, and SATCOM.

DIOGO MARINHO (Member, IEEE) was born in Aveiro, Portugal, in 1993. He received the M.Sc. degree in electronic and telecommunications engineering from the Universidade de Aveiro, Aveiro, Portugal, in 2018, where he is currently pursuing the Ph.D. degree in electrical engineering with the Department of Electronics, Telecommunications and Informatics. In September 2018, he joined the Instituto de Telecomunicações. His research interests include software defined radio, digital beamforming, radar, 5G, microwave filters, and mmWave.

TIAGO VARUM (Member, IEEE) was born in Estarreja, Portugal, in 1987. He received the M.Sc. degree in electronic and telecommunications engineering and the Ph.D. degree in electrical engineering from the Universidade de Aveiro, Aveiro, Portugal, in 2010 and 2016, respectively. He is currently a Research Assistant with the Instituto de Telecomunicações, Aveiro. He has participated in some projects, published several articles in this field, in conference proceedings and journals. His current research interests include antenna design, reconfigurable antennas, 3D-printed antennas, non-uniform antenna arrays, beamforming, and smart/adaptive antennas, for mmWave applications (radar, 5G, or SATCOM).

Dr. Tiago is a member of the IEEE Antennas and Propagation Society. He has been a reviewer of several journals and international conferences.

JOÃO NUNO MATOS (Member, IEEE) was born in Oliveira de Azeméis, Portugal, in 1959. He received the degree in electronic and telecommunications engineering from the Universidade de Aveiro, Aveiro, Portugal, in 1982, the master's degree in electrical science from the University of Coimbra, Portugal, in 1989, and the Ph.D. degree in electrical engineering from the Universidade de Aveiro, in 1995. From 1982 to 1983, he worked twice in the industry with Portugal Telecom Innovation, Aveiro. In 1990, he was with Ensa Electronic, Madrid, Spain. From 1998 to 2000, he was the Head of the Electronics and Telecommunications Department, Universidade de Aveiro, where he is currently an Associate Professor and also a Senior Researcher with the Instituto de Telecomunicações. He has authored or coauthored more than 100 international conference papers and journals. With the Instituto de Telecomunicações, he participated or led dozens of research's projects in RF/microwave (MW) circuits, system design, and system integration. His current research interests include satellite communications and radars with a special focus on front-end and smart antennas, and engineering education.

Dr. Matos is a member of several scientific committees of conferences and journals, and professional organizations. He is currently on the Executive Committee of the IEEE Portugal Education Chapter (2019 IEEE Education Society Chapter Achievement Award).